Generation and detection of alkyl peroxy radicals in a supersonic jet expansion

H. B. Fu, Y. J. Hu, and E. R. Bernstein

Citation: The Journal of Chemical Physics **125**, 014310 (2006); doi: 10.1063/1.2209680
View online: http://dx.doi.org/10.1063/1.2209680
View Table of Contents: http://aip.scitation.org/toc/jcp/125/1
Published by the American Institute of Physics

Generation and detection of alkyl peroxy radicals in a supersonic jet expansion

H. B. Fu, Y. J. Hu, and E. R. Bernstein
Department of Chemistry, Colorado State University, Fort Collins, Colorado 80523-1872

(Received 14 March 2006; accepted 9 May 2006; published online 5 July 2006)

Alkyl peroxy radicals are synthesized in a supersonic jet expansion by the initial production of alkyl radicals and subsequent reaction with molecular oxygen. Parent ions CH_3OO^+/CD_3OO^+ are observed employing vacuum ultraviolet (VUV) single photon ionization/time-of-flight mass spectroscopy (TOFMS). Employing infrared (IR)+VUV photofragmentation detected spectroscopy, rotationally resolved infrared spectra of jet-cooled CH_3OO and CD_3OO radicals are recorded for the $\tilde{A}\,^2A' \leftarrow \tilde{X}\,^2A''$ transition by scanning the IR laser frequency while monitoring the CH_3^+ and CD_3^+ ion signals generated by the VUV laser. The band origins of the $\tilde{A}\,^2A' \leftarrow \tilde{X}\,^2A''$ transition for CH_3OO and CD_3OO are identified at 7381 and 7371 cm^{-1}, respectively. Rotational simulation for the CH_3OO and CD_3OO 0_0^0 transitions of $\tilde{A} \leftarrow \tilde{X}$ yields a rotational temperature for these radicals of ~30 K. With the aid of *ab initio* calculations, two and five vibrational modes for the $\tilde{A}\,^2A'$ excited electronic state are assigned for CH_3OO and CD_3OO radicals, respectively. Both experimental and theoretical results suggest that the ground electronic state of the ions of ethyl and propyl peroxy radicals are not stable although their ionization energies (IE) are less than 10.5 eV. The $C_2H_5OO^+/C_3H_7OO^+$ cations can readily decompose to $C_2H_5^+/C_3H_7^+$ and O_2. This is partially responsible for the inability of IR+VUV photofragmentation spectroscopy to detect the near IR $\tilde{A} \leftarrow \tilde{X}$ electronic transition for these radicals. © *2006 American Institute of Physics*.
[DOI: 10.1063/1.2209680]

I. INTRODUCTION

Alkyl peroxy radicals, ROO, play critically important roles as reaction intermediates in atmospheric oxidation[1–3] and low temperature combustion[4–6] of hydrocarbons. In the troposphere, hydrocarbon oxidation is initiated by hydrogen abstraction by the hydroxyl radical followed by the association with molecular oxygen to form ROO. The subsequent fate of alkyl peroxy radicals, either by self-reaction or reaction with atmospheric species, such as NO, NO_2, SO_2…, has been the subject of many kinetic studies.[7–10] For instance, the formation of the tropospheric ozone,[11,12] can occur through

$$\mathrm{ROO} + \mathrm{NO} \rightarrow \mathrm{RO} + \mathrm{NO_2}, \tag{1}$$

$$\mathrm{NO_2} + \mathrm{h}\nu(\mathrm{Sun}) \rightarrow \mathrm{NO} + \mathrm{O}(^3P), \tag{2}$$

$$\mathrm{O_2} + \mathrm{O}(^3P) + \mathrm{M} \rightarrow \mathrm{O_3} + \mathrm{M}. \tag{3}$$

In low temperature flames, the competition between hydrocarbon radical reactions with O_2 to form peroxy radicals, and hydrocarbon radical self-reaction is critical to the amount of soot production.[13] Formation of ROO followed by isomerization to hydroperoxy and alkyl radicals is the dominant reaction pathway for the activation of hydrocarbons.[6]

Historically, most studies of alkyl peroxy radical reactions have employed UV absorption spectroscopy to monitor the $\tilde{B}\,^2A'' \leftarrow \tilde{X}\,^2A''$ transition centered at ~240 nm that is common to all alkyl peroxy radicals.[1,12] The $\tilde{B}\,^2A'' \leftarrow \tilde{X}\,^2A''$ transition of ROO is broad and unstructured due to the repulsive nature of the $\tilde{B}$ state. The quasicontinuum nature of this transition makes it inapplicable for obtaining rotational or vibrational information about ROO, in general. Additionally, the overlapping of the UV spectra of different alkyl peroxy radicals makes the identification of a specific one, particularly from a mixture, a great challenge. The $\tilde{A}\,^2A' \leftarrow \tilde{X}\,^2A''$ transition of ROO in the near IR does display resolved vibrational and rotational spectra as reported by Hunziker *et al.* using a modulation absorption technique[14] and by Miller *et al.* using cavity ring down spectroscopy.[15–19] Characterization of the $\tilde{A}\,^2A'' \leftarrow \tilde{X}\,^2A''$ transitions of peroxy radicals not only yields information on their properties and reactivities, but also provides a sensitive and selective technique for their detection. This near IR transition has a small transition cross section ($\sigma \sim 10^{-21}$–10^{-22} cm^2); however, our recent results for supersonic beam samples combined with IR+VUV (118 nm) photofragmentation detected (PFD-IR) spectroscopy of the alkyl peroxy radical have proven that the IR+VUV PFD-IR approach is sensitive enough to detect the $\tilde{A}\,^2A' \leftarrow \tilde{X}\,^2A''$ transitions of alkyl peroxy radicals.[20]

In the present study, alkyl peroxy radicals are synthesized in a supersonic jet expansion by the initial production of alkyl radicals and subsequent reaction with molecular oxygen. Parent ions CH_3OO^+ and CD_3OO^+ are observed by 10.5 eV single photon ionization/time-of-flight mass spectroscopy (TOFMS). Vibrationally resolved spectra of jet-cooled CH_3OO and CD_3OO radicals are recorded for the $\tilde{A}\,^2A' \leftarrow \tilde{X}\,^2A''$ transition by means of the IR+VUV PFD-IR

spectroscopy. Simulations of the partially resolved rotational structure for a number of vibronic features in this transition yield a radical rotational temperature of ~30 K for CH_3OO in the electronic ground state. Based on *ab initio* calculations, two and five vibrational modes in the $\tilde{A}\,^2A'$ state are assigned for CH_3OO and CD_3OO, respectively. No parent ions of ethyl or propyl peroxy radicals are observed employing 10.5 eV single photon ionization/TOFMS. Calculations suggest that cations of ethyl and propyl peroxy radicals are unstable, and that $C_2H_5OO^+/C_3H_7OO^+$ cations can easily decompose to $C_2H_5^+/C_3H_7^+$ and O_2. This is partially responsible for the inability of IR+VUV PFD-IR techniques to yield spectra for the $\tilde{A}\,^2A' \leftarrow \tilde{X}\,^2A''$ transitions of these species.

II. EXPERIMENT

A. Generation of alkyl peroxy radicals

To the best of our knowledge, the only report of the generation of peroxy radicals in a supersonic expansion is documented in Ref. 20 for acetyl peroxy radicals. In the present study, alkyl peroxy radicals are generated by the initial production of an alkyl radical with subsequent three-body reaction with molecular oxygen prior to supersonic expansion into a vacuum system. Photolysis of acetone and/or its deuterated analog at 193 nm is used to generate the methyl radical. The reaction mechanism is likely

$$CH_3COCH_3/CD_3COCD_3 + h\nu(193\ \text{nm}) \rightarrow 2CH_3/CD_3 + CO, \quad (4)$$

$$CH_3/CD_3 + O_2 + M \rightarrow CH_3OO/CD_3OO + M. \quad (5)$$

A mixture of 3% spectroscopic grade acetone or acetone-d_6 (Aldrich) and 30% O_2 (99.9%, General Air) in helium (99% General Air) at a backing pressure of ~60 psi is expanded into the vacuum chamber through a 0.5 mm orifice of a Parker General Valve Series 9 pulsed solenoid valve. A pulsed ArF laser at 193 nm (Lambda Physik, 8 mJ/pulse) is focused by a cylindrical lens with a 1 m focal length into the middle of a quartz tube (1 mm i.d. and 2 cm long) attached to the face plate of the nozzle in line with the 0.5 mm orifice. Acetone has a large absorption cross section at 193 nm, $\sigma \sim 10^{-17}$ cm^2.

Dissociation of acetone at 193 nm produces only the methyl radical and CO.[21,22] Sample contact time in the quartz tube is estimated between 50 and 100 μs.[23] O_2 concentration is as high as 30%, which is sufficient to assure rapid conversion of CH_3 to CH_3OO [reaction (5)].

The ethyl and propyl peroxy radicals are generated by photolysis of Cl_2 as 355 nm in a mixture of 2% Cl_2, 5% ethane or propane, and 30% O_2 in He, according to the reactions

$$Cl_2 + h\nu(355\ \text{nm}) \rightarrow 2Cl, \quad (6)$$

$$Cl + C_2H_6/C_3H_8 \rightarrow C_2H_5/C_3H_7 + HCl, \quad (7)$$

$$C_2H_5/C_3H_7 + O_2 + M \rightarrow C_2H_5OO/C_3H_7OO + M. \quad (8)$$

The experimental set up is similar to that described for the synthesis of methyl peroxy radical except that the photolysis laser source is now 355 nm, generated by tripling the output of a Nd/YAG laser. Molecular chlorine has a cross section at this wavelength for photolysis $\sim 2\times10^{-19}$ cm^2.[24] Equations (6)–(8) portray the reaction steps in this synthesis.[25]

B. Radical detection

Peroxy radicals of interest (ROO, $R=C_nH_{2n+1}$) produced in the quartz tube at the exit of the pulsed nozzle or in the collisional part of the molecular beam, undergo cooling during supersonic expansion. The molecular beam from the nozzle is collimated by a 1.5 mm diameter skimmer (Beam Dynamics), located 2.5 cm downstream from the nozzle exit, and then crossed perpendicularly by the VUV (118 nm) laser (ionization) beam in the ionization region of the TOFMS. The counter-propagating (to the 118 nm beam) IR laser pump beam is focused upstream (1 to 2 mm) from the VUV laser focal point by a 40 cm focal length lens.

Generation of the VUV (118 nm) laser radiation is similar to that used in our metal oxide cluster studies.[26] Employing 25 mJ/pulse of 355 nm light from a tripled Nd/YAG laser and 200 Torr of a 1:10 mixture of Xe–Ar, 118 nm radiation is generated at about 1 μJ/pulse or ~10^{12}photons/pulse. Tunable IR radiation is obtained from an optical parametric oscillator (OPO-Laser Vision) pumped by an injection seeded Nd/YAG laser (Spectra Physics). A type II KDP (KH_2PO_4) doubling crystal is integrated into the OPO laser converting the Nd/YAG laser fundament output to 532 nm. Two interchangeable sets of nonlinear crystals in the system are used to produce the outputs that provide wavelength coverage from 712 to 2130 nm. For both oscillator configurations, the output beam consists of both signal and idler wavelengths from the down conversion of the 532 nm pump, and a birefringent polarizer (CPBA—10.0, CVI Laser Corp.) is used to separate them. The OPO laser output between 4760 and 7800 cm^{-1} has a pulse energy of ~4 mJ/pulse and a bandwidth of ~0.4 cm^{-1}. The output between 7800 and 10 990 cm^{-1} has a pulse energy of ~10 mJ/pulse and a bandwidth of ~2 cm^{-1}.

Ions created by the VUV ionization laser are extracted by a 250 V potential and accelerated in the TOFMS to 4 keV total kinetic energy. Mass resolved detection is achieved by a Galileo Electro-Optics multichannel plate (MCP) at the end of a 1.5 m flight tube. The pulsed nozzle and three lasers are operated at 10 Hz and synchronized by two digital delay generators (SRS DG535, Stanford Research Systems). Data acquisition scheme for infrared spectroscopy is similar to that used to record resonance enhanced multiphoton ionization (REMPI) spectroscopy described in detail in previous publications.[27,28] Recently, IR/VUV ionization spectroscopy has been exploited to study IR absorption of molecules, clusters,[29] and radicals[20] in this laboratory. The possible mechanisms for the detection of alkyl peroxy radicals using IR+VUV PFD-IR spectroscopy are discussed in detail below.

TABLE I. The molecular geometries for ROO in the neutral $\tilde{X}\,^2A''$, netural $\tilde{A}\,^2A'$, and ionic $\tilde{X}\,^3A''$ states, together with the $\tilde{A}\,^2A' \leftarrow \tilde{X}\,^2A''$ transition and ionization energies for ROO, calculated at the B3LYP/aug-cc-pVDZ level of theory.

	C-OO (Å)			O-O (Å)			Energy of $\tilde{A} \leftarrow \tilde{X}$ (cm^{-1})	Ionization energy (eV)
ROO	$\tilde{X}\,^2A''$	$\tilde{A}\,^2A'$	lon $\tilde{X}\,^3A''$	$\tilde{X}\,^2A''$	$\tilde{A}\,^2A'$	lon $\tilde{X}\,^3A''$		
CH_3OO	1.452	1.440	1.513	1.317	1.385	1.201	7459	10.80
CD_3OO							7449	
C_2H_5OO	1.466	1.453	1.605	1.316	1.383	1.197	7597	10.44
C_3H_7OO	1.464	1.452	1.612	1.316	1.383	1.197	7552	10.35

III. RESULTS AND DISCUSSION

A. Theory

To support our mass and IR spectroscopic observations, we have performed density-functional theory (DFT) calculations on alkyl peroxy radicals using the GAUSSIAN 98 series of programs.[30] The B3LYP hybrid density functional is employed in conjunction with the correlation-consistent Dunning basis set of double-ζ quality (aug-cc-pVDZ) to calculate optimized molecular structures, rotational constants, and harmonic vibrational modes.

Since supersonic expansion cools the species in the molecular beam via collisions with the inert carrier gas, only low energy conformers for alkyl peroxy radicals are considered to be populated. Methyl peroxy has two conformers: One is a trans form with the OO group staggered with respect to the methyl group H-atoms; and the other conformer is a cis form with the terminal O and a methyl H eclipsed. The latter is known to be a saddle point on the CH_3OO ground electronic state potential energy surfaces[31] and this is further confirmed by the present calculation. Recent calculations[32] have shown two stable conformers for C_2H_5OO: Trans (T) and gauche (G) forms corresponding to 0° and 120° for the dihedral angle between the O–O–C and O–C–C planes, respectively. Only the spectrum of the T isomer of C_2H_5OO has been observed, even at room temperature.[14] In the case of C_3H_7OO, two isomeric forms are identified: 1-propyl and 2-propyl peroxy radicals. For 1-propyl peroxy, the lowest energy conformer has a geometry T_1T_2 with T_1 (G_1) specifying the dihedral angle between O–O–C and O–C–C planes, and T_2 (G_2) specifying the angle between the O–C–C and C–C–C planes.[16,17]

All three lowest energy conformers for methyl, ethyl, and 1-propyl peroxy radicals have C_s symmetry. They have a ROO $\tilde{X}\,^2A''$ ground electronic state, a ROO $\tilde{A}\,^2A'$ first excited electronic state, and ROO^+ $\tilde{X}\,^3A''$ ion ground electronic state. Before optimizing the geometry for the first excited ROO state $\tilde{A}\,^2A'$, an excited-state calculation at the CIS/aug-cc-pVDZ level is always completed in order to determine the β orbitals that are involved in the $\tilde{A}\,^2A' \leftarrow \tilde{X}\,^2A''$ electronic transition. Table I summarizes the major bond changes for ROO in the neutral ground electronic state ROO $\tilde{X}\,^2A''$, the neutral first excited state ROO $\tilde{A}\,^2A'$, and the ionic ground electronic state ROO^+ $\tilde{X}\,^3A''$. Energies for the $\tilde{A}\,^2A' \leftarrow \tilde{X}\,^2A''$ transition, as well as the ionization energy in each case, are obtained using the zero point corrected electronic state energies. The two neutral states have nearly the same geometry but the ionic ground state geometry is quite different. Upon ionization for all ROO species considered, the bond length r(C–OO) increases while the r(O–O) bond length decreases. The O–O bond length in the ion $\tilde{X}\,^3A''$ state is almost equal to that of molecular oxygen calculated at the same theory level. The C–OO bond is still computer drawn for the CH_3OO^+ but is not drawn for the $C_2H_5OO^+$ and 1-$C_3H_7OO^+$ ions. Thus, the latter two radicals are probably unstable in the ion ground state.

B. Methyl peroxy radical spectra

Figure 1 shows the VUV single photon ionization TOFMS of Figs. 1(a) and 1(c) 3% acetone, 30% O_2 in He and Fig. 1(b) 3% acetone in He. Figure 1(a) is recorded as a blank with the photolysis laser off. Features appear at m/z =58 amu due to $CH_3COCH_3^+$ (very strong, not shown here), m/z=43 amu due to CH_3CO^+ (strong), and at m/z =15 amu due to CH_3^+ (weak) for Figs. 1(a) and 1(c). The feature at m/z=16 is probably O^+ in Figs. 1(a) and 1(c): It arises because of the 193 nm laser in Fig. 1(c), but in Fig. 1(a) it probably is associated with residual 355 nm radiation. The ionization energy (IE) of CH_3COCH_3 is 9.7 eV, and the

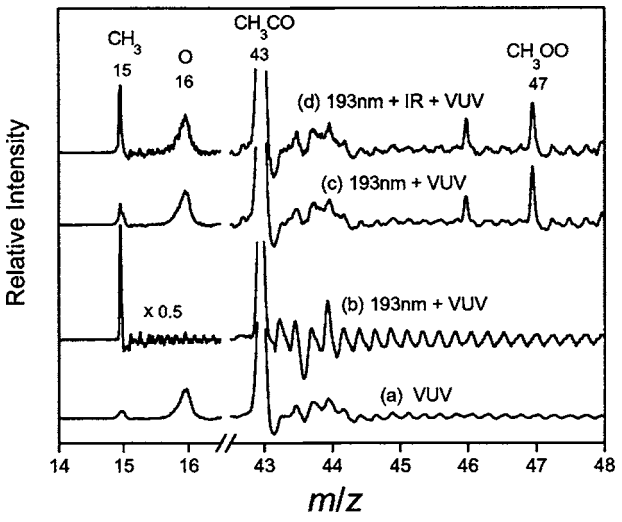

FIG. 1. VUV single photon ionization/TOFMS spectra of (a) and (c) 3% acetone, 30% O_2, in helium, and (b) 3% acetone in helium. Spectrum (a) is recorded with the 193 nm photolysis laser is blocked, while traces (b) and (c) are recorded with the 193 nm photolysis laser light present.

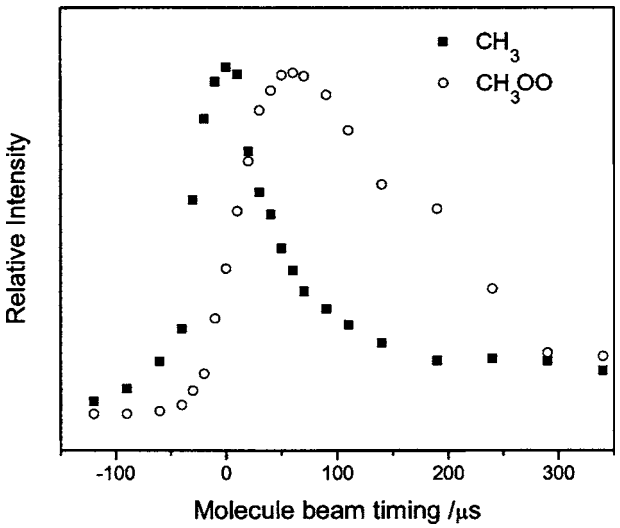

FIG. 2. Molecular beam timing of CH_3 and CH_3OO obtained by adjusting the timing for the VUV ionization laser and monitoring the CH_3^+ and CH_3OO^+ intensity. Timing for the pulsed nozzle and 193 nm photolysis laser is fixed.

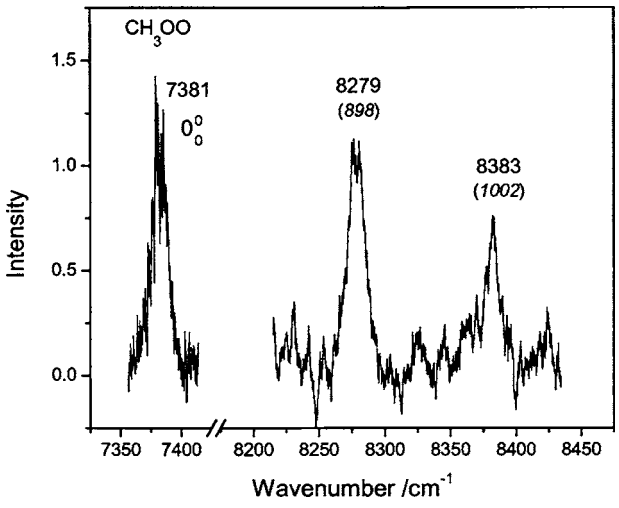

FIG. 3. Infrared spectrum of jet-cooled CH_3OO for the $\tilde{A}\,^2A' \leftarrow \tilde{X}\,^2A''$ transition recorded by PFD-IR spectroscopy with monitoring the CH_3^+ at $m/z=15$ mass channel signal.

appearance energies for CH_3CO^+ and CH_3^+ from CH_3COCH_3 are 10.3 and 15.2 eV, respectively.[33] When the photolysis laser (193 nm) is turned on, a strong increase in the CH_3^+ signal at $m/z=15$ is observed in Fig. 1(b) for the 3% CH_3COCH_3/He sample. In Fig. 1(c) (sample 3% CH_3COCH_3/30% O_2/He), a peak at $m/z=47$ clearly emerges while the signal intensity of the CH_3^+ channel decreases. The presence of both photolysis light at 193 nm and O_2 is necessary for the appearance of the CH_3OO^+ feature at $m/z=47$ amu: This latter feature is thereby assigned as the parent ion of the methyl peroxy radical formed through reactions (4) and (5). The consumption of CH_3 in reaction (5) results in the decrease in the concentration of CH_3 in the molecular beam. Comparing Figs. 1(b) (no O_2) and 1(c) (O_2), the CH_3^+ intensity decreases by almost 75% for the sample with O_2 present. Moreover, CD_3OO^+ signal at $m/z=50$ amu is also present if acetone-d_6 is employed as the precursor molecule.

Figure 2 shows the molecular beam timing for the arrival CH_3 and CH_3OO at the ionization region. This flight time difference arises from the mass of the two species and the inability of the He carrier gas to accelerate them both to the beam speed (average speed of He at 300 K), and the extra time needed to synthesize CH_3OO from CH_3 and O_2. The time difference for the peak intensity between CH_3 and CH_3OO is roughly 60 μs, but note that when CH_3 is at about 90% maximum intensity, CH_3OO is near 10% maximum intensity.

With the molecular beam timing fixed for the CH_3OO maximum intensity, introduction of an IR laser beam at 7382 cm^{-1}, ~30 ns prior to the VUV laser beam, leads to an increase of CH_3^+ intensity by almost a factor of 3, as shown in Fig. 1(d), over that found in Fig. 1(c). If the molecular beam timing is fixed for the CH_3 maximum intensity without IR present, the presence of IR radiation at the ionization region does not change the CH_3^+ intensity at the $m/z=15$ amu. This implies that the CH_3^+ intensity increases in Fig. 1(d) with respect to that in Fig. 1(c) induced by the addition of IR radiation, relates to the presence of CH_3OO in the molecular beam. Observing the affect of IR radiation in mass channel 15, rather than mass channel 47, clearly should generate a much better signal/noise ratio for the CH_3OO IR $\tilde{A}\,^2A' \leftarrow \tilde{X}\,^2A''$ spectrum.

The calculated results suggest that the CH_3OO^+ ion may be unstable, and can decompose into CH_3^+ and O_2 depending on the excess energy released into CH_3OO^+ during the ionization process. Since the VUV photon energy (10.5 eV) is just near the ionization threshold of CH_3OO (calculated IE =10.8 eV), the excess energy is low for CH_3OO^+ ionized from the ground state $\tilde{X}\,^2A''$ state of CH_3OO. CH_3OO $\tilde{A}\,^2A' \leftarrow \tilde{X}\,^2A''$ transition has a 0_0^0 absorption at 7381 cm^{-1},[15] and around 1 eV of excess energy exists in CH_3OO^+ ionized by a VUV photon from the $\tilde{A}\,^2A'$ state rather than the $\tilde{X}\,^2A''$ state. This extra energy will dissociate CH_3OO^+ to yield CH_3^+ and an increased signal intensity in the $m/z=15$ amu mass channel. Large Franck-Condon factors between the $\tilde{A}\,^2A'$ state of the neutral and vibronic combination bands of the cation may increase the ionization efficiency for the IR +VUV detection scheme.[34] Therefore, in IR/VUV PFD-IR spectroscopy detection of the $\tilde{A}\,^2A' \leftarrow \tilde{X}\,^2A''$ transition for the methyl peroxy radical is achieved by scanning the IR laser frequency while monitoring the mass channel intensity belonging to the photo fragment CH_3^+ at $m/z=15$ with the appropriate photolysis/ionization laser timing.

Figure 3 presents a survey of the PFD-IR spectrum of CH_3OO^+ for the $\tilde{A}\,^2A' \leftarrow \tilde{X}\,^2A''$ transition. The band centered at 7381 cm^{-1} is attributed to the origin of the transition 0_0^0. The features at 8279 and 8381 cm^{-1} are vibronic transition from the 0_0 level to excited $^2A'$ state vibrations. In the spectral region around the 0_0^0 transition, the IR OPO has an output linewidth of 0.4 cm^{-1} and thus some rotational structure can be resolved for this transition. Employing the rotational constants calculated for the trans conformer of CH_3OO (see

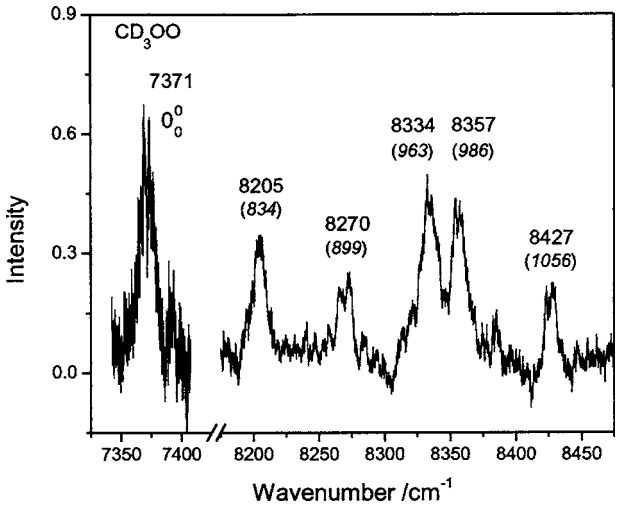

FIG. 4. Infrared spectrum of jet-cooled CD_3OO for the $\tilde{A}\,^2A' \leftarrow \tilde{X}\,^2A''$ transition recorded by PFD-IR spectroscopy with monitoring the CD_3^+ at $m/z = 18$ mass channel signal.

Table I in the supporting material[38]), the 0_0^0 $\tilde{A}\,^2A' \leftarrow \tilde{X}\,^2A''$ transition can be simulated (see Figure 1S in the supporting material[38]) using the SPECVIEW software package.[35] The rotational temperature that best fits the observed band structure is $T_{\mathrm{rot}} \sim 30$ K. The band origin is determined to be at 7381 ± 1 cm^{-1}, consistent with the published values.[15] No further efforts have been made to refine these rotational constants because our resolution (laser linewidth) does not generate a line to line assignment of rotational levels. The two active vibrational modes in the $^2A'$ state appear at 898 and 1002 cm^{-1} above the 0_0^0 transition.

Photolysis of acetone-d_6 has also been carried out and the CD_3OO spectrum arising from this sample, treated and presented in the same manner as discussed above, is shown in Fig. 4. The 0_0^0 $\tilde{A}\,^2A' \leftarrow \tilde{X}\,^2A''$ transition for CD_3OO is determined at 7371 ± 1 cm^{-1} through a rotational simulation of the observed envelope structure (see Figure 2S in the supporting material[38]) using the SPECVIEW software package.[35] As shown in Table I, this redshift of the 0_0^0 band center upon deuteration of the methyl peroxy radical is predicted by the calculations. Figure 4 reveals five active vibrational modes for CD_3OO in the excited $\tilde{A}\,^2A'$ state, with energies 834, 899, 963, 986, and 1056 cm^{-1}. These modes and those found for CH_3OO $\tilde{A}\,^2A'$ are listed in Table II. The possible tentative assignments of these features are also listed in Table II based on our B3LYP/aug-cc-pVDZ calculations of harmonic vibrational mode energies.

Methyl peroxy has a plane of symmetry passing through all heavy atoms and one hydrogen atom. This C_s symmetry species possesses 12 normal modes, eight of A' symmetry and four of A'' symmetry.[36] Local modes can be thought of as derived from a H_3C-X molecule: R_1 the symmetric stretch, R_2 the umbrella mode, R_3 the degenerate stretch, R_4 the degenerate deformation, and R_5 the degenerate rock.[36] In the C_s molecule, R_3R_4, R_5 split into A' and A'' modes. Since only A' modes are allowed from the $\tilde{X}\,^2A''(0_0)$ level in the $\tilde{A} \leftarrow \tilde{X}$ transition, we consider only A' modes in the discussion of the vibronic transitions of the $\tilde{A} \leftarrow \tilde{X}$ spectrum.

The two active modes observed in the $\tilde{A} \leftarrow \tilde{X}$ CH_3OO transition are at 898 and 1002 cm^{-1} and they are of comparable energies to those reported in Ref. 37 from anion photo-detachment photo-electron spectra (PES) as $\nu_s = 910 \pm 10$ cm^{-1} and $\nu_t = 1005 \pm 9$ cm^{-1}. One can assign these two modes to the harmonic vibrations $\omega_7 = 917$ and $\omega_6 = 1015$ cm^{-1} from our calculations (see Fig. 3 and Table II). *Ab initio* calculations suggest that the $\tilde{A}$ state vibrations of CH_3OO are unlike the local modes observed for the $\tilde{X}$ state, in that the $\tilde{A}$ state normal modes involve significant local mode mixing. Anion photo-detachment photo-electron spectroscopy can identify two normal modes for CD_3OO, $\nu_s = 840 \pm 120$ and $\nu_t = 975 \pm 10$ cm^{-1}.[37] Our feature at 834 cm^{-1} is comparable to the ν_s feature in PES,[37] red shifted by 64 cm^{-1} from that observed for CH_3OO and as calculated for ω_7. The mode is a D_3C-O-O or H_3C-O-O symmetric stretch. The feature at 975 cm^{-1} in the PES spectrum, resolves to two features in the IR spectrum at 963 and 986 cm^{-1}. The feature at 963 cm^{-1} should be the ω_7—a nor-

TABLE II. UB3LYP/aug-cc-pVDZ harmonic frequencies and experimental values for the $\tilde{A}\,^2A'$ state of the methyl peroxy radical. All assignments are tentative, as they are based only on the calculated energies for the identified $\tilde{A}$ state modes.

Mode a'	Local mode	CH_3OO $\tilde{A}\,^2A'$ ($T_\infty = 7381$ cm^{-1}) Cal	P.E.[a]	This work exp.	CD_3OO $\tilde{A}\,^2A'$ ($T_\infty = 7371$ cm^{-1}) Cal	P.E.[a]	This work exp.
ω_1	R_{3a}	3157			2342		
ω_2	R_1	3025			2164		
ω_3	R_{4a}	1475			1069		**986**
ω_4	R_2	1419			1087		**1056**
ω_5	R_{5a}+OO	1157			950		**899**
ω_6	R_{5a}-OO	1015	1005[a]	**1002**	1007	975[a]	**963**
ω_7	H_3C-OO stretch	917	910[a] 896[b]	**898**	836	840[a]	**834**
ω_8	H_3C-O-O bend	370			343		

[a]From Ref. 37.
[b]From Ref. 14.

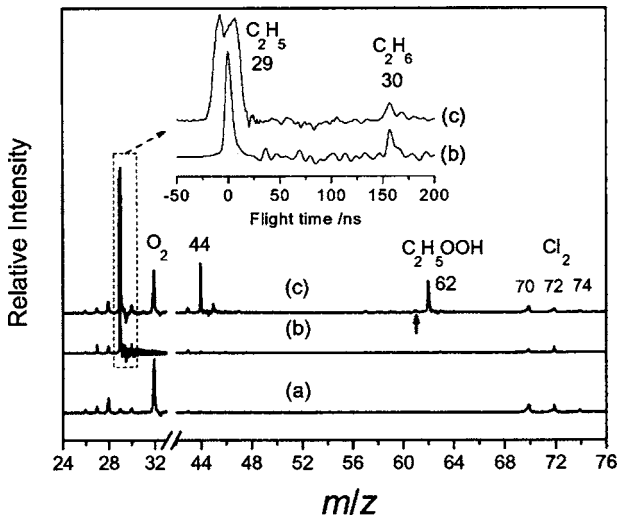

FIG. 5. VUV single photon ionization/TOFMS spectra of (a) and (c) 2% Cl_2, 5% C_2H_6, 30% O_2 in helium, and (b) 2% Cl_2, 5% C_2H_6 in helium. Spectrum (a) is recorded with the 355 nm photolysis laser is blocked, while traces (b) and (c) are recorded with the 355 nm photolysis laser light present. The inset shows the time-of-flight peak profile of $C_2H_5^+$ cation. The arrow indicates mass channel 61 at which the $C_2H_5OO^+$ cation is expected.

mal mode combination of the CD_3 rock and O–O stretch. The feature at 986 cm^{-1} should be ω_3—a normal mode combination of a CD_3 deformation and O–O stretch. Additionally, the feature at 899 cm^{-1} is probably ω_5 and the feature at 1056 cm^{-1} we suggest is ω_4. The unpaired electron on the methyl peroxy radical is localized on the terminal oxygen atom, and hence modes involving this atom are expected to be most active in the $\tilde{A} \leftarrow \tilde{X}$ transition. Indeed, the DFT calculations suggest that motion of the deutrated methyl group has more influence on the motion of the O–O group than the CH_3 group does, simply because CD_3 is heavier than CH_3. Unfortunately, our laser output between 7800 and 10 990 cm^{-1} has a bandwidth of 2 cm^{-1}, and this resolution does not allow for the rotational analysis of transitions located in this spectral range. Our assignments for these vibrational modes must, therefore, be tentative.

C. C_2H_5OO and 1-C_3H_7OO

Figure 5 displays the TOFMS obtained by single photon ionization at 10.5 eV with Figs. 5(a) and 5(c) 2% Cl_2, 5% C_2H_2, 30% O_2 in He, and Fig. 5(b) 2% Cl_2, 5% C_2H_5 in He. Figure 5(a) has no 355 nm photolysis at the nozzle, while Figs. 5(b) and 5(c) have this laser radiation present at the nozzle quartz tube. Figure 5(a) serves as a blank sample. [An O_2^+ ion is observed in Figs. 5(a) and 5(c) probably due to two photon absorption of either 118 nm light plus residual 355 nm light from 118 nm generation or of 118 nm light. Note that O_2 is in very high concentration in the beam, and that the intensity of the 118 nm light and residual 355 nm light is similar at the ionization focal point for our optical set up.][26] Features belonging to $C_2H_3^+$ and Cl_2^+ can be identified in Fig. 5(a) but are very weak. The IE $(Cl_2)=11.48$ eV, IE $(O_2)=12.07$ eV, and IE $(C_2H_6)=11.5$ eV[33] are all above the 10.5 eV single photon energy: 355 nm light has a single photon energy of 3.49 eV, so 10.5+3.49 eV can create the referenced ions. With the presence of 355 nm light at the nozzle, reaction (6) is initiated and $C_2H_5^+$ is generated by reaction (7) as is presented in Fig. 5(b). The IE $(C_2H_5)=8.2$ eV,[33] and recall that Fig. 5(b) has no O_2. In the presence of the molecular O_2 and 355 nm photolysis light for Cl_2, one expects to observe C_2H_5OO; however, Fig. 5(c) is complicated, with peaks at $m/z=44$ and 62, and the peak at $m/z=61$ for $C_2H_5OO^+$ is very weak. The DFT calculations presented in Table I indicate that a VUV photon at 10.5 eV should be energetic enough to ionize C_2H_5OO; however, they also show that $C_2H_5OO^+$ is unstable and can readily decompose to $C_2H_5^+$ and O_2. As shown in the insert spectra for Fig. 5, the full width at half maximum (FWHM) of the $C_2H_5^+$ peak in the absence of O_2 [Fig. 5(b)] is 10 ns (the FWHM of the laser pulse at 118 nm), whereas the FWHM of this feature with O_2 present is ~30 ns with an unresolved doublet shape. This suggests that the $C_2H_5^+$ observed in the presence of O_2 in the sample is fragmented from a larger species and has excess kinetic energy: For example, from $C_2H_5OO^+$. We have observed similar, although more extreme, behavior for the photodissociation of CH_3I detected by CH_3^+. Mass peaks at $m/z=44$ and 62 in Fig. 5(c) can be associated with CH_3CHO and C_2H_5OOH, which are reported as products from the self-reaction of C_2H_5OO radicals.[1]

Results obtained for a sample containing C_3H_8 as a precursor for the generation of C_3H_7OO radicals clarify that $C_3H_7OO^+$ is also unstable and can readily decompose to $C_3H_7^+$ and O_2 (see Figure 3S in the supporting material[38]). Unfortunately, the IR+VUV PFD-IR technique does not yield spectra for either ethyl or propyl peroxy radicals, perhaps because the ions ROO^+ are unstable and their dissociation masks the IR induced generation of R^+ or because the absorbed IR energy does not significantly alter the cross section for ionization. Note too that the IR spectra of C_2H_5OO and C_3H_7OO are both broad and weak.[15–19]

IV. CONCLUSIONS

We have observed the production of methyl, ethyl, and propyl peroxy radicals in a supersonic jet expansion by the initial generation of alkyl radicals and their subsequent reaction with O_2. Parent ions of CH_3OO and CD_3OO are observed using 10.5 eV single photon ionization/TOFMS. Vibrationally resolved spectra of expansion cooled CH_3OO and CD_3OO are recorded for the $\tilde{A}\,^2A' \leftarrow \tilde{X}\,^2A''$ transition by scanning the IR laser frequency while monitoring the CH_3^+/CD_3^+ ions signals produced by a VUV laser. The origin bands for the $\tilde{A}\,^2A' \leftarrow \tilde{X}\,^2A''$ transitions for CH_3OO and CD_3OO are at 7381 and 7371 cm^{-1}, respectively. Rotational simulation results for the 0_0^0 transitions show a rotational temperature for these radicals ~30 K. Combined with DFT calculations, two and five vibrational modes for the $\tilde{A}\,^2A'$ excited electronic states of CH_3OO and CD_3OO, respectively, are observed and tentatively assigned. No parent ions for ethyl and propyl peroxy radicals are observed using 10.5 eV single photon ionization/TOFMS. DFT calculation results suggest that the ion ground states of these radicals are unstable.

ACKNOWLEDGMENTS

This work was supported by grants from U.S. NSF and Philip Morris International through the Research Management Group.

[1] T. J. Wallington, P. Dagaut, and M. J. Kurylo, Chem. Rev. (Washington, D.C.) **92**, 667 (1992).
[2] B. J. Finlayson-Pitts, and J. N. Pitts, Jr., Science **276**, 1045 (1997).
[3] P. D. Lightfoot, R. A. Cox, J. N. Crowley, M. Destriau, G. D. Hayman, M. E. Jenkin, G. K. Moortgat, and F. Zabel, Atmos. Environ., Part A **26**, 1805 (1992).
[4] S. W. Benson, J. Am. Chem. Soc. **87**, 972 (1965).
[5] S. Wang, D. L. Miller, N. P. Cernansky, H. J. Curran, W. J. Pitz, and C. K. Westbrook, Combust. Flame **118**, 415 (1999).
[6] H. J. Curran, P. Gaffuri, W. J. Pitz, and C. K. Westbrook, Combust. Flame **114**, 149 (1998).
[7] R. Lesclaux, in *Peroxyl Radicals*, edited by Z. B. Alfassi (Wiley, New York, 1997), p. 92.
[8] M. D. King, and K. C. Thompson, Atmos. Environ. **37**, 4517 (2003).
[9] A. Masaki, S. Tsunashima, and N. Washida, Chem. Phys. Lett. **218**, 523 (1994).
[10] J. H. Xing, Y. Nagai, M. Kusuhara, and A. Miyoshi, J. Phys. Chem. A **108**, 10458 (2004).
[11] B. J. Finlayson-Pitts, and J. N. Pitts, Jr., in *Atmospheric Chemistry* (Wiley, New York, 1986).
[12] T. J. Wallington and O. J. Nielson, in *Peroxy Radicals* (Wiley, New York, 1997), p. 72.
[13] A. D'Anna, A. Violi, and A. D'Alessio, Combust. Flame **121**, 418 (2000).
[14] H. E. Hunziker and H. R. Wendt, J. Chem. Phys. **64**, 3488 (1976).
[15] M. B. Pushkarsky, S. J. Zalyubovsky, and T. A. Miller, J. Chem. Phys. **112**, 10695 (2000).
[16] S. Zalyubovsky, B. Glover, T. A. Miller, C. Hayes, J. K. Merle, and C. M. Hadad, J. Phys. Chem. A **109**, 1308 (2005).
[17] G. Tarczay, S. Zalyubovsky, and T. A. Miller, Chem. Phys. Lett. **406**, 81 (2005).
[18] S. J. Zalyubovsky, B. G. Glover, and T. A. Miller, J. Phys. Chem. A **107**, 7704 (2003).
[19] B. G. Glover, and T. A. Miller, J. Phys. Chem. A **109**, 11191 (2005).
[20] Y. J. Hu, H. B. Fu, and E. R. Bernstein, J. Phys. Chem. A **110**, 2629 (2006).
[21] J. C. Owrutsky and A. P. Baronavski, J. Chem. Phys. **110**, 11206 (1999).
[22] S. W. North, D. A. Blank, D. J. Gezelter, C. A. Longfellow, and Y. T. Lee, J. Chem. Phys. **102**, 4447 (1995).
[23] H. B. Fu, Y. J. Hu, and E. R. Bernstein, J. Chem. Phys. **123**, 234307 (2005).
[24] D. Maric, J. P. Burrows, R. Meller, and G. K. Moortgat, J. Photochem. Photobiol., A **70**, 205 (1993).
[25] J. S. Pilgrim, A. McIlroy, and C. A. Taatjes, J. Phys. Chem. A **101**, 1873 (2003).
[26] D. N. Shin, Y. Matsuda, and E. R. Bernstein, J. Chem. Phys. **120**, 4150 (2004).
[27] R. Disselkamp and E. R. Bernstein, J. Chem. Phys. **98**, 4339 (1993).
[28] E. R. Bernstein, K. Law, and M. Schauer, J. Chem. Phys. **80**, 207 (1984).
[29] H. B. Fu, Y. J. Hu, and E. R. Bernstein, J. Chem. Phys. **124**, 024302 (2006).
[30] GAUSSIAN 98 Rev. A. 11, M. J. Frisch, G. W. Trucks, H. B. Schlegel *et al.*, (Gaussian, Inc., Pittsburgh PA, 2001).
[31] J. A. Jafri and D. H. Phillips, J. Am. Chem. Soc. **112**, 2586 (1990).
[32] J. C. Rienstra-Kiracofe, W. D. Allen, and H. F. S. Schaefer, J. Phys. Chem. A **104**, 9823 (2000).
[33] The NIST Chemistry Webbook http://webbook.nist.gov/chemistry
[34] X. M. Qian, A. H. Kung, T. Zhang, K. C. Lau, and C. Y. Ng, Phys. Rev. Lett. **91**, 233001 (2003).
[35] V. L. Stakhursky, http://molspect.mps.ohio-state.edu/goes/specview.html
[36] S. Nandi, S. J. Blanksby, X. Zhang, M. R. Nimlos, D. C. Dayton, and G. B. Ellison, J. Phys. Chem. A **106**, 7547 (2002).
[37] S. J. Blanksby, T. M. Ramond, G. E. Davico, M. R. Nimlos, S. Kato, V. M. Bierbaumb, W. C. Lineberger, G. B. Ellison, and M. Okumura, J. Am. Chem. Soc. **123**, 9585 (2001).
[38] See EPAPS Document No. E-JCPSA6-124-007624 for rotational constants and simulated spectra of methyl peroxy radicals, and mass spectra obtained for a sample containing C_3H_8 as a precursor for the generation of C_3H_7OO radicals. This document can be reached via a direct link in the online article's HTML reference section or via the EPAPS homepage (http://www.aip.org/pubservs/epaps.html).